Journal of Innovative Optical Health Sciences
Vol. 9, No. 6 (2016) 1650002 (9 pages)

DOI: 10.1142/S1793545816500024

Near-infrared chemical imaging for quantitative analysis of chlorpheniramine maleate and distribution homogeneity assessment in pharmaceutical formulations

Manfei Xu, Luwei Zhou, Qiao Zhang, Zhisheng Wu*,‡, Xinyuan Shi and Yanjiang Qiao†,‡
Beijing University of Chinese Medicine, P. R. China 100102

Pharmaceutical Engineering and New Drug Development of Traditional Chinese Medicine (TCM) of Ministry of Education, P. R. China 100102

Key Laboratory of TCM-information Engineering of State Administration of TCM Beijing, P. R. China 100102

Beijing Key Laboratory for Basic and Development Research on Chinese Medicine Beijing, P. R. China 100102
**wzs@bucm.edu.cn*
†yjqiao@263.net

Received 19 January 2015
Accepted 14 May 2015
Published 29 June 2015

Near infrared chemical imaging (NIR-CI) combines conventional near infrared (NIR) spectroscopy with chemical imaging, thus provides spectral and spatial information simultaneously. It could be utilized to visualize the spatial distribution of the ingredients in a sample. The data acquired using NIR-CI instrument are hyperspectral data cube (hypercube) containing thousands of spectra. Chemometric methodologies are necessary to transform spectral information into chemical information. Partial least squares (PLS) method was performed to extract chemical information of chlorpheniramine maleate in pharmaceutical formulations. A series of samples which consisted of different CPM concentrations (w/w) were compressed and hypercube data were measured. The spectra extracted from the hypercube were used to establish the PLS model of CPM. The results of the model were R^2_{val} 0.981, RMSEC 0.384%, RMSECV 0.483%, RMSEP 0.631%, indicating that this model was reliable.

Keywords: Near infrared chemical imaging; partial least squares regression; assessment of distributional homogeneity; chlorpheniramine maleate.

‡Corresponding authors.

1. Introduction

Near infrared chemical imaging (NIR-CI) is an emerging technique which combines conventional near infrared (NIR) spectroscopy with chemical imaging to provide spectral and spatial information simultaneously.[1] Traditional single point NIR spectroscopy obtains a bulk average spectrum to reflect an average composition of the sample. NIR-CI adds a spatial dimension to NIR spectroscopy, which gifts NIR-CI ability to acquire distributional information of ingredients in the sample.

In NIR-CI, the spectrum of the sample is recorded and finally all spectra comprise a hyperspectral data cube.[2] Once the spectral signature of each pixel was transferred into chemical information (i.e., the concentration), the chemical images will be generated, which reflect the distribution of components in the sample. NIR-CI also owns the superiorities of being rapid, nondestructive and without sample pretreatment. Therefore, NIR-CI has the potential to acquire increasing process and product understanding, which is consistent with the process analytical technology (PAT)[3] initiative encouraged by Food and Drug Administration (FDA) in pharmaceutical field.

The ability of simultaneously obtaining spectral and spatial information of components has made NIR-CI a promising PAT tool for the control of pharmaceutical manufacturing process and quality assessment of final products. The applications of NIR-CI include the assessment of homogeneity of mixture during the blending process,[4–7] the visualization of spatial distribution of components in intermediate and final product,[8,9] the discrimination of counterfeit pharmaceutical products,[10–12] etc. More pharmaceutical applications of NIR-CI technique can refer to previous reviews.[13,14] Among the applications, NIR-CI is especially suitable to assess distribution homogeneity of component in the sample, as spatial information could be acquired by NIR-CI.

However, the data measured by NIR-CI are three-dimensional hypercube. All the ingredients spectral signatures are overlapping and chemometric methods are required to obtain relevant qualitative or quantitative information. The hypercube could be analyzed by either three-way method or the two-way method. It was proved that the two-way methods were more suitable for this type of data.[15] The hypercube has to be unfolded to two-dimensional matrix and then conventional two-way methodologies could be used. The most commonly used methods include the univariate methods (i.e., the characteristic wavenumber method) and multivariate methods, such as partial least squares (PLS), classical least squares and so on. Finally, the two-dimensional matrix is refolded to retain the spatial distribution of each pixel and reconstruct the chemical images.

Chlorpheniramine maleate (CPM) is a H1 receptor antagonist and has a strong action of anti-histamine.[16] It has been clinically used to alleviate symptoms of cold and treat the allergic disease. According to the Chinese pharmacopoeia (2010 Edition, Volume II), legitimate labeled content of CPM in CPM tablets is 1 mg or 4 mg. The CPM content is about 1–5% (w/w) in a tablet. Active pharmaceutical ingredient (API) distribution plays an important role in both medicine safety and efficacy, especially for small dose products or sustained and controlled release products. Therefore, it is necessary to assess the distributional homogeneity of CPM in the tablet. In this study, the CPM tablets made by ourselves were taken as examples. NIR-CI was used to acquire the concentration information of CPM coupled with PLS method. Then, the concentration value reconstruction images were generated for further distributional homogeneity assessment.

2. Materials and Methods

2.1. *Materials*

A four-ingredient pharmaceutical tablet formulation was used to produce the NIR-CI data set. The API of tablet was CPM and provided by Haohua Industry Corporation (Jinan, P. R. China). The main excipients of the tablet were pregelatinized starch (STA) and microcrystalline cellulose (MCC), which were purchased from Colorcon (USA) and Beijing FengliJingqiu Commerce and Trade Corporation (P. R. China), respectively. Magnesium stearate (MgS) was purchased from Sinopharm Chemical Reagent Corporation (P. R. China) and served as lubricant.

2.2. *Sample preparation*

The calibration data set comprised of 33 batches was designed by a D-optimal formulation design using Design Expert 7.0 software (USA). The

content range of CPM was from 1% to 10%, and 20% to 90% for pregelatinized starch and from 10% to 80% for MCC. The content of magnesium stearate was fixed because a little amount was added extra in the formulation (0.4%, w/w). Table 1 showed the contents of the four ingredients in each of the 33 calibration batches.

The mixing of dry-blend formulation was performed in a blender using the equal incremental method and compressed into tablets of 0.5 g by direct compression on a rotary tablet press (Xinyuan Pharmaceutical Machinery Corporation, Shanghai, P. R. China). The parameters of rotary tablet press were set as compression pressure 60 KN, the depth of filling material 5.0 mm and the thickness of the tablet 2.0 mm. A flat punch was utilized to obtain a flat sample surface. Besides, three batches of prediction set were produced in the same way to test the performance of the PLS model. The ingredients contents of prediction set were also demonstrated in Table 1. The CPM contents in the prediction set were 4.5%, 5.5% and 6.5%, which were within the content range of the calibration set in PLS model.

Table 1. The content of components of each batch (w/w).

Number	CPM	STA	MCC	MgS
Calibration set				
1	0.099	0.239	0.662	0.004
2	0.086	0.812	0.100	0.004
3	0.024	0.525	0.451	0.004
4	0.010	0.302	0.688	0.004
5	0.050	0.228	0.722	0.004
6	0.074	0.464	0.462	0.004
7	0.066	0.578	0.356	0.004
8	0.018	0.882	0.100	0.004
9	0.045	0.652	0.303	0.004
10	0.047	0.701	0.252	0.004
11	0.010	0.477	0.513	0.004
12	0.036	0.366	0.597	0.004
13	0.010	0.765	0.225	0.004
14	0.100	0.400	0.500	0.004
15	0.014	0.200	0.786	0.004
16	0.083	0.517	0.400	0.004
17	0.100	0.302	0.598	0.004
18	0.099	0.716	0.185	0.004
19	0.052	0.785	0.164	0.004
20	0.099	0.606	0.295	0.004
21	0.064	0.700	0.276	0.004
22	0.053	0.495	0.452	0.004
23	0.011	0.389	0.600	0.004
24	0.010	0.475	0.510	0.004
25	0.020	0.470	0.505	0.004
26	0.030	0.465	0.500	0.004
27	0.040	0.460	0.495	0.004
28	0.050	0.455	0.490	0.004
29	0.060	0.450	0.485	0.004
30	0.070	0.445	0.480	0.004
31	0.080	0.440	0.475	0.004
32	0.090	0.435	0.470	0.004
33	0.100	0.430	0.465	0.004
Prediction set				
1	0.045	0.51	0.432	0.013
2	0.055	0.50	0.432	0.013
3	0.065	0.49	0.432	0.013

2.3. *Hyperspectral data acquisition*

One tablet from start, middle and the end of the tableting process of each batch was selected in order to assure a representative sampling for calibration set. Therefore, a total of 99 samples were imaged (3 tablets from each of the 33 calibration batches). For the three batches in prediction set, one tablet of each batch was compressed and imaged.

Each sample was fixed onto a microscope slide and detected directly on the tablet surface. A NIR lining mapping instrumentation (Spotlight 400N FT-NIR Imaging Systems, PerkinElmer, UK) was applied to analyze the samples. A linear mercury cadmium telluride (MCT) array detector enables 16 spectra being collected in one measurement. An area ($1000\,\mu m \times 1000\,\mu m$ for calibration set and $2000\,\mu m \times 2000\,\mu m$ for prediction set) was imaged using pixel size $25\,\mu m \times 25\,\mu m$ and spectrum resolution $16\,cm^{-1}$ thus acquiring a total of 1600 spectra for calibration set and 6400 for prediction set for each image. Each spectrum was the average of 16 scans and the wavenumber region was from 7800 to $4000\,cm^{-1}$.

A high reflectance standard Spectralon TM (Labsphere, Inc., North Sutton, New Hampshire) was used as a background to correct the instrument response. Hence, relative NIR diffuse reflectance data ($R = R_{sample}/R_{background}$) could be obtained and transferred into absorbance data ($A = -lg(1/R)$) for further analysis.

2.4. *Data processing*

The NIR-CI data is a hyperspectral data cube ($M = X \times Y \times \lambda$, X and Y represent spatial dimensions and λ is spectral dimension). Commonly, the three-dimensional matrix would be unfolded

into two-dimensional matrix ($XY \times \lambda$) and then two-way methodologies could be performed.

Though multivariate approaches can analyze the spectral data using the entire measured wavenumber range, proper variable selection could improve the precision of a multivariate method in some cases. SiPLS was utilized to select the optimal wavenumber ranges for PLS models.

Besides, proper preprocessing methods were used to avoid the impact of nonchemical information from the image. In this study, some most commonly used approaches were used, such as Savitzkky–Golay (SG) derivative transformation, multiplicative scatter correction (MSC) and standard normal variate (SNV).[17]

2.5. *PLS modeling and image reconstruction*

PLS is a multivariate regression methodology performed to construct quantitative calibration model. This method is based on the relation between the spectral signals (X) and the reference values (Y).[18] The spectral data would be corrected to a property matrix of maintaining the information of interest while removing interference signal of other spectral factors.

In this study, PLS model of the active pharmaceutical ingredient (CPM) was established. A total of 99 calibration samples were imaged and the mean spectrum of each sample was computed. Then, the three mean spectra of each batch were averaged. The 33 mean spectra of calibration batch comprised the matrix X. The theoretical content (%, w/w) formed the matrix Y for each component. The sample set was divided by Kennard–Stone (KS) algorithm into calibration set (22 samples) and validation set (11 samples). PLS model was constructed and optimized according to the number of latent factors, preprocessing methods and wavenumber range calculated from the regression model. Leave-one-out cross validation was utilized as cross-validation approach.

After the same pretreatments, the hypercube data of the prediction set was applied to the built PLS model. Several parameters are used to assess the predictive capability of PLS model, such as the determination coefficient (R^2), root mean square error of calibration (RMSEC), root mean square error of cross validation (RMSECV) and root mean square error of prediction (RMSEP).

Then, the spectral information of each pixel would be converted into predicted concentration information. The concentration image of CPM was generated through the reconstruction of predicted concentration matrix retaining the spatial location of each pixel. The mean concentration of CPM was calculated by averaging all predicted pixel concentrations.

Hyper View software and Spectrum Image software (PerkinElmer, UK) were used for data processing and analysis. Other data analysis was performed by home-made routines programmed in MATLAB software (MATLAB2009b, Mathworks, USA).

2.6. *Assessment of distributional homogeneity of CPM*

After NIR-CI measurement and data analysis, the spatial distribution images of components could be obtained. Through observing the distribution images by eyes, the homogeneity of ingredient could be preliminarily assessed. However, this method is not objective and it is difficult to quantitatively assess the homogeneity of different samples.

A criterion called "distributional homogeneity index (DHI)" has been proposed to assess the distributional homogeneity of chemical image. This method was based on continuous-level moving block (CLMB) methodology and calculating the ratio of areas under the real and random homogeneity curve of chemical images. The distribution is more homogeneous, the value of DHI is closer to 1. Through the calculation of DHI value, the distribution homogeneity of different samples could be objectively assessed. More detail descriptions of the DHI theory could be found in Ref. 19.

3. Results and Discussion

3.1. *PLS modeling*

3.1.1. *Data preprocessing*

The three-dimensional data obtained from NIR-CI equipment was unfolded into two-dimensional matrix. The spectra would be affected by the overlapping peaks, spectral noise or baseline drift, etc. Preprocessing approaches were performed to improve the accuracy of the model performance.

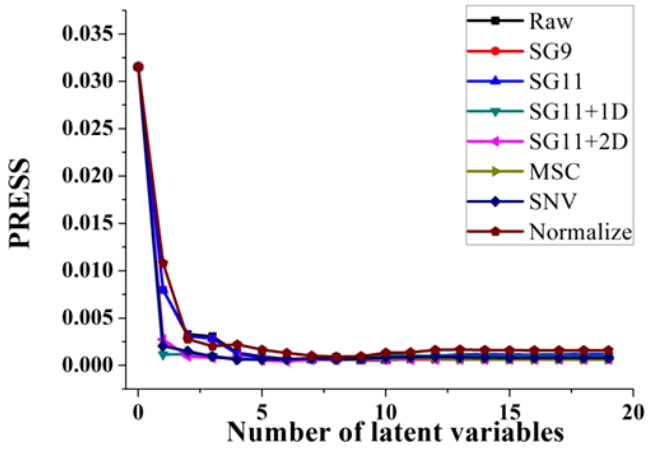

Fig. 1. PRESS plot of CPM with different pretreatment methods.

Several types of preprocessing approaches were utilized in the spectral dataset, such as origin spectra, SG smoothing with 9-point window, SG smoothing with 11-point window, 11-point SG and first derivative (SG+1D), 11-point SG and second derivative (SG+2D), SNV, MSC and normalize. Leave-one-out cross validation was used to select the optimal preprocessing method and the number of latent variable factors was investigated.

The optimum number of latent variable factors was obtained by calculating the lowest predicted residual sum of squares (PRESS) value, because the minimal PRESS value indicates a good balance between the robustness of the model and R^2 value. Finally, a plot of latent factors against press value was generated by the model, as seen in Fig. 1. The result of PLS models with different pretreatment methods were demonstrated in the Table 2. The spectra preprocessed by 11-point SG and second derivative methodology had the lowest latent factors, RMSECV value and coefficient of determination (R^2) value closest to 1, which was proved to be the best preprocessing method for PLS model.

3.1.2. *Variable selection by SiPLS model*

Moreover, SiPLS was utilized as a variable selection method. The dataset of full spectrum was separated into several intervals. Several intervals were used to build a joint model and the RMSECV value was regarded as the measure of the accuracy of models. The combination of intervals with the lowest RMSECV was chosen. Using this method, the spectral regions that have poor information about the property in study are eliminated while that important bands are retained, thus decreasing the vulnerability of the calibration models.[20] With variable selection for characteristic spectral regions, the performance of previous PLS model may be improved in this way.

In this paper, the SiPLS model was constructed with combination of subinterval number 3 using 10 equidistant subintervals and 2 factors. The RMSECV, RMSEP and RMSEC were 0.574%, 0.648%, 0.416%, respectively, which indicated low performance of SiPLS model. It was because the full spectrum contained more information needed in this situation. Therefore, the calibration set of full spectrum was used as matrix X to build PLS model directly.

3.1.3. *Establishment of PLS model*

Based on the above analysis, the spectra preprocessed by 11-point SG and 2 derivate were used to build PLS model with 2 latent factors. The RMSECV, RMSEP and RMSEC were 0.483%, 0.631% and 0.384%, respectively. The R^2 were all higher than 0.9, indicating a good accuracy of PLS

Table 2. Different pretreatment methods of PLS model.

Preprocessing methods	Latent factors	RMSEC (%)	R^2_{cal}	RMSECV (%)	R^2_{val}	RMSEP (%)	R^2_{pre}
Raw	4	0.527	0.977	0.707	0.962	0.838	0.897
SG9	4	0.481	0.981	0.638	0.969	0.712	0.926
SG11	4	0.480	0.981	0.635	0.969	0.670	0.929
SG11+1D	2	0.443	0.983	0.615	0.981	0.696	0.929
SG11+2D	2	0.384	0.988	0.483	0.982	0.631	0.941
MSC	3	0.617	0.968	0.850	0.945	0.738	0.920
SNV	3	0.617	0.968	0.851	0.950	0.739	0.920
Normalize	4	0.571	0.973	0.733	0.959	0.729	0.922

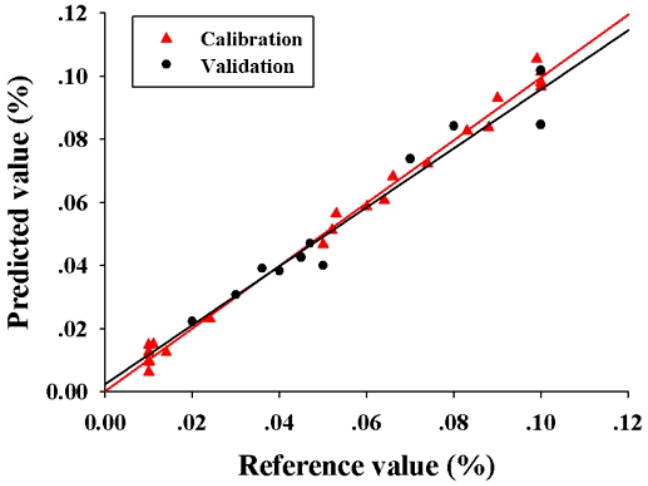

Fig. 2. CPM NIR predictions versus the reference result.

model. Figure 2 demonstrated the calibration and validation regressions for PLS model, the reference value and prediction value almost distributed in a straight line closely. The parameters of PLS model for API indicated that this model was reliable.

3.2. *Quantification and chemical image reconstruction*

One tablet sample for each batch in prediction set was measured and analyzed with the method as described in Secs. 2.5 and 3.1, respectively. A total of 6400 spectra were acquired for each sample ($(2000 \times 2000)/(25 \times 5) = 6400$, an area of $2000\,\mu\text{m} \times 2000\,\mu\text{m}$, spatial resolution $25\,\mu\text{m} \times 25\,\mu\text{m}$). Each spectrum was applied to the built PLS model and concentration of each pixel could be predicted.

Figure 3 showed the concentration images of the three samples in prediction set. The images were reconstructed based on the predicted concentration of each pixel according to the origin spatial location. The color band from blue to red represented the range of concentration from low to high. Thus, the spatial distribution of API can be illustrated and visualized. The mean concentration of each component was calculated by averaging all predicted concentrations of pixels. The mean concentration of each sample was 4.09%, 5.95% and 5.85%, respectively.

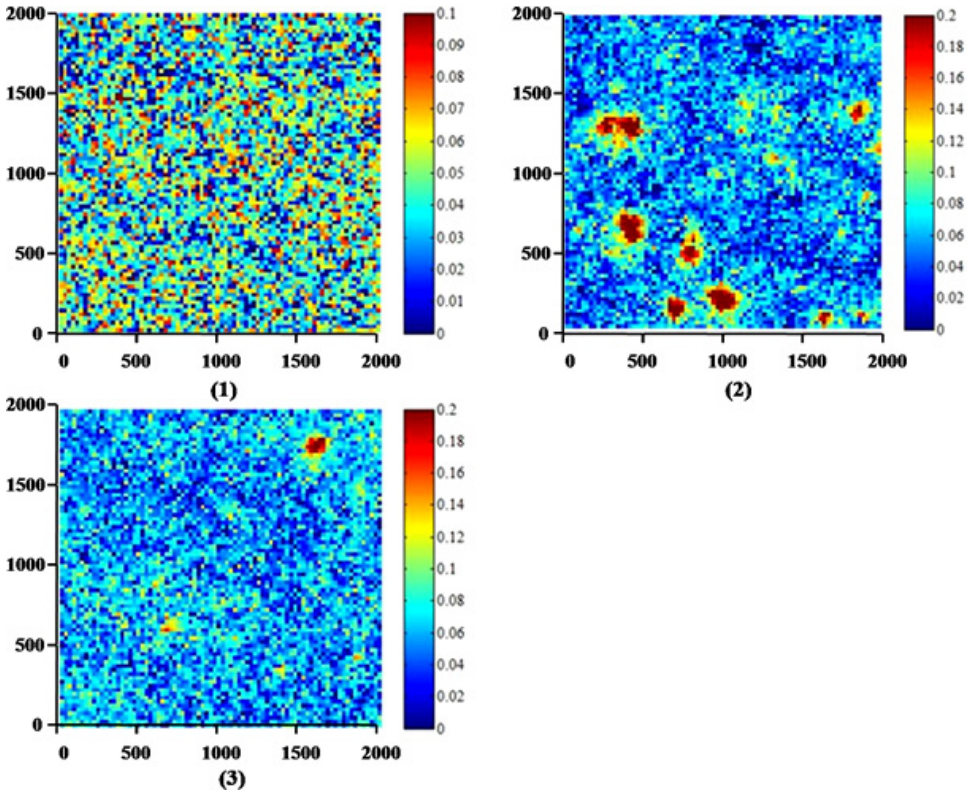

Fig. 3. Concentration value of reconstruction images of three samples in prediction set (1) Sample 1, (2) Sample 2, (3) Sample 3.

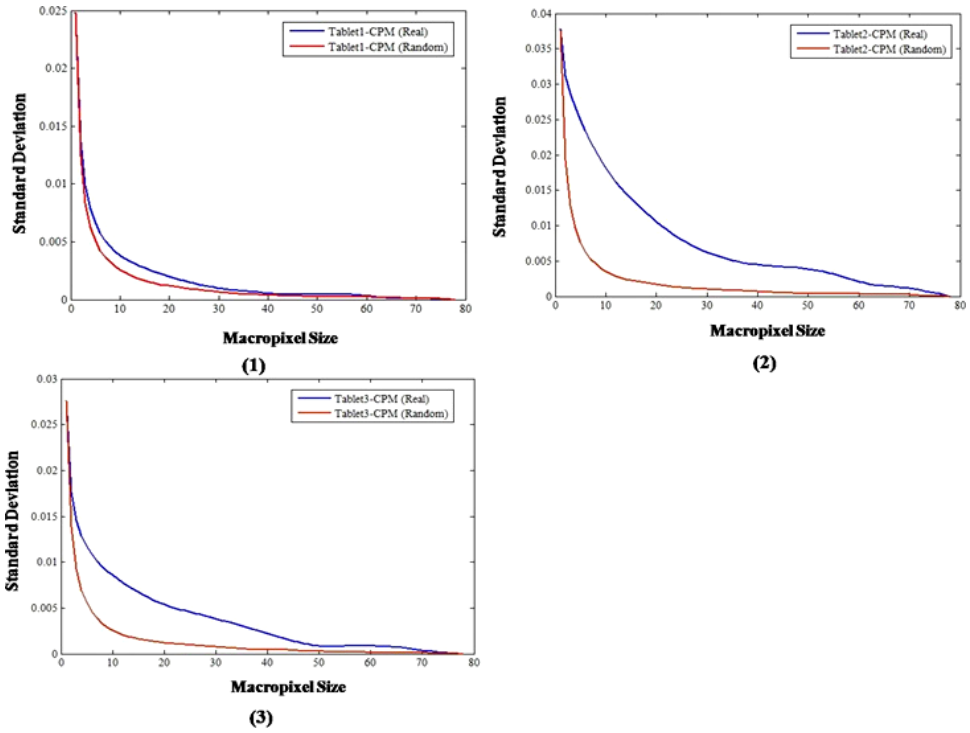

Fig. 4. Homogeneity curve of CPM distribution of three samples in prediction set. (1) Sample 1, (2) Sample 2, (3) Sample 3; DHI = AUC_{real}/AUC_{random}.

3.3. *Assessment of distributional homogeneity of CPM*

As shown in Fig. 3, CPM distribution of sample 1 was dispersive and homogeneous by eyes. Nevertheless, there were some large red areas could be observed on the surface of sample 2 and sample 3, which indicated the existence of aggregation and agglomeration phenomenon of CPM. Through visual observation, CPM distribution of sample 1 was considered to be the most homogeneous while CPM distribution of sample 2 might be the most inhomogeneous.

However, the assessment of CPM distribution might be subjective only by naked eyes. Hence, DHI method was performed to further assess the CPM distributional homogeneity of different samples. The size of concentration value reconstruction images of CPM was 80 pixel × 80 pixel. Therefore, the image was sampled by the different sizes of macropixels from 2 pixel × 2 pixel to 80 pixel × 80 pixel.

First, the standard deviation (Std) of each size of macropixel of real concentration reconstruction image was computed. Second, the real concentration reconstruction image was randomized to generate its corresponding random image. Similarly, the random image was sampled by different sizes of macropixels and the Std value of each size of macropixel was calculated. Then, the homogeneity curve of real distribution image and random distribution image was drawn through plotting Std value against macropixel size (Fig. 4). Ultimately, the area under the homogeneity curve (real and random) was calculated and the value of DHI was obtained.

The DHI value of each sample was 1.394, 4.300 and 2.635, respectively. The tablet becomes more homogeneous as the DHI value increases. Therefore, the CPM distributional homogeneity of sample 1 was the most ideal while the distribution of sample 2 was the most inhomogeneous.

4. Conclusions

NIR-CI can acquire spatial distribution information of components in a sample besides providing spectral information. Through unfolding the hypercube into two-dimensional matrix, conventional two-way

chemometric approaches could be used to extract interested chemical image. In this study, PLS method was performed to acquire concentration information of CPM tablets. A total of 33 mean spectra and the theoretical CPM contents of each batch were used as matrix X and Y to establish the PLS model. The data matrix of prediction set was applied to the PLS model and the spectral information was transferred into concentration information. The CPM concentration value reconstruction images were generated through refolding the two-dimensional matrix according to the origin spatial location of each pixel. A criterion called DHI was performed to assess the CPM distributional homogeneity of different samples. The result indicated that the sequence of CPM distributional homogeneity of 3 samples was: sample 1, sample 3, sample 2.

NIR-CI has showed great potential in pharmaceutical industry as an emerging PAT tool. With the help of chemometrics, the measured spectral information could be transformed into chemical information. Moreover, the spatial information could be also obtained. The ability of providing distributional information makes it especially suitable to assess homogeneity of components in the sample. More attention should be paid to NIR-CI and more efforts should be made to promote its development.

Acknowledgments

This work was financially supported from Beijing Municipal Government for the university affiliated with the Party Central Committee (Prof. Shi), National Natural Science Foundation of China (81303218), Doctoral Fund of Ministry of Education of China (20130013120006), Special Fund of Beijing University of Chinese Medicine (Manfei Xu).

Manfei Xu and Luwei Zhou contributed equally to this work.

References

1. G. Reich, "Near-infrared spectroscopy and imaging: Basic principles and pharmaceutical applications," *Adv. Drug Deliv. Rev.* **57**, 1109–1143 (2005).
2. G. P. Sabin, M. C. Breitkreitz, A. M. de Souza, P. da Fonseca, L. Calefe, M. Moffa, R. J. Poppi. "Analysis of pharmaceutical pellets: An approach using near-infrared chemical imaging," *Anal. Chim. Acta* **706**, 113–119 (2011).
3. D. C. Hinz, "Process analytical technologies in the pharmaceutical industry: The FDA's PAT initiative," *Anal. Bioanal. Chem.* **384**, 1036–1042 (2006).
4. A. S. El-Hagrasy, H. R. Morris, F. D'Amico, R. A. Lodder, J. K. 3 rd. Drennen, "Near-infrared spectroscopy and imaging for the monitoring of powder blend homogeneity," *J. Pharm. Sci.* **90**, 1298–1307 (2001).
5. H. Ma, C. A. Anderson, "Characterization of pharmaceutical powder blends by NIR chemical imaging," *J. Pharm. Sci.* **97**, 3305–3320 (2008).
6. T. Furukawa, H. Sato, H. Shinzawa, I. Noda, S. Ochiai, "Evaluation of homogeneity of binary blends of poly (3-hydroxybutyrate) and poly (L-lactic acid) studied by near infrared chemical imaging (NIRCI)," *Mater. Charact.* **23**, 871–876 (2007).
7. Z. S. Wu, O. Tao, X. X. Dai, M. Du, X. Y. Shi, Y. J. Qiao, "Monitoring of a pharmaceutical blending process using near infrared chemical imaging," *Vib. Spectrosc.* **63**, 371–379 (2012).
8. L. W. Zhou, Z. S. Wu, X. Y. Shi, M. F. Xu, X. N. Liu, B. Xu, Y. J. Qiao, "Rapid discrimination of chlorpheniramine maleate and assessment of its surface content uniformity in a pharmaceutical formulation by NIR-CI coupled with statistical measurement," *J. Spectrosc.* **2014** (2014).
9. A. Palou, J. Cruz, M. Blanco, J. Tomàs, J. de los. Ríos, M. Alcalà, "Determination of drug, excipients and coating distribution in pharmaceutical tablets using NIR-CI," *J. Pharm.* **2**, 90–97 (2012).
10. O. Y. Rodionova, L. P. Houmoller, A. L. Pomerantsev, P. Geladi, J. Burger, V. L. Dorofeyev, A. P. Arzamastsev. "NIR spectrometry for counterfeit drug detection: A feasibility study," *Anal. Chim. Acta* **549**, 151–158 (2005).
11. J. Dubois, J. C. Wolff, J. K. Warrack, J. Schoppelrei, E. N. Lewis, "NIR chemical imaging for counterfeit pharmaceutical products analysis," *Spectroscopy* **22**, 40 (2007).
12. M. B. Lopes, J. C. Wolff, "Investigation into classification/sourcing of suspect counterfeit Heptodin (TM) tablets by near infrared chemical imaging," *Anal. Chim. Acta* **633**, 149–155 (2009).
13. A. A. Gowen, C. P. O'Donnell, P. J. Cullen, S. E. J. Bell, "Recent applications of chemical imaging to pharmaceutical process monitoring and quality control," *Eur. J. Pharm. Biopharm.* **69**, 10–22 (2008).
14. C. Gendrin, "Chemical imaging and chemometrics for the analysis of pharmaceutical solid dosage forms," Engineering Sciences (Physics), Université Louis Pasteur-Strasbourg I (2008).
15. J. Huang, H. Wium, K. B. Qvist, K. H. Esbensen, "Multi-way methods in image analysis — relationships

and applications," *Chemometr. Intell. Lab.* **66**, 141–158 (2003).
16. J. Kirkegaard, C. Secher, N. Mygind, "Effect of the H1 antihistamine chlorpheniramine maleate on histamine — Induced symptoms in the human Conjunctiva," *Allergy* **37**, 203–208 (1982).
17. J. M. Amigo, J. Cruz, M. Bautista, S. Maspoch, J. Coello, M. Blanco, "Study of pharmaceutical samples by NIR chemical image and multivariate analysis," *TrAC. Trend. Anal. Chem.* **27**, 696–713 (2008).
18. C. Ravn, E. Skibsted, R. Bro, "Near-infrared chemical imaging (NIR-CI) on pharmaceutical solid dosage forms — Comparing common calibration approaches," *J. Pharm. Biomed.* **48**, 554–561 (2008).
19. P. Y. Sacré, P. Lebrun, P. F. Chavez, C. D. Bleye, L. Netchacovitch, E. Rozet, R. Klinkenberg, B. Streel, P. Hubert, E. Ziemons, "A new criterion to assess distributional homogeneity in hyperspectral images of solid pharmaceutical dosage forms," *Anal. Chim. Acta* **818**, 7–14 (2014).
20. M. F. Ferrão, M. D. S. Viera, R. E. P. Pazos, D. Fachini, A. E. Gerbase, L. Marder, "Simultaneous determination of quality parameters of biodiesel/diesel blends using HATR-FTIR spectra and PLS, iPLS or siPLS regressions," *Fuel* **90**, 701–706 (2011).